


Article

Dynamics Model of a Multi-Rotor UAV Propeller and Its Fault Detection

Yongtian Zou, Haiting Xia , Xinmin Yang * , Peigen Li and Yu Yi

Faculty of Civil Aviation and Aeronautics, Kunming University of Science and Technology, Kunming 650500, China; zyt181@stu.kust.edu.cn (Y.Z.); haiting.xia@kust.edu.cn (H.X.); peigenli@stu.kust.edu.cn (P.L.); 20242245024@stu.kust.edu.cn (Y.Y.)

* Correspondence: xinminyang@kust.edu.cn

Abstract: The propeller state of unmanned aerial vehicles (UAV) is difficult to detect in real time due to trouble with laying out the sensor and multiple signal sources. To solve this problem, a fault detection method for multi-rotor UAV propellers was proposed based on a signal analysis of the built-in inertial measurement unit (IMU). Firstly, the multi-source coupled signals of the UAV flight were obtained through the ground station. Then, the picked-up signals were optimally separated according to the multi-rotor UAV propeller fault dynamics model, and signals rich in fault information were obtained. Finally, the separated signals were calculated using the symmetrized dot pattern (SDP), and then the similarity index was used to quantify the distribution of the signal in the feature plot to realize propeller fault detection. The OTSU algorithm was used to quantify the detection results, yielding a similarity of 76.2% in the z-axis direction, which is better than the values in the other two directions. The simulation and experimental analysis of the propeller failure dynamics model showed that the proposed method can effectively identify the propeller faults of multi-rotor UAVs.

Keywords: unmanned aerial vehicle; inertial measurement unit; symmetrized dot pattern; fault detection



Academic Editor: Mostafa Hassanalain

Received: 1 January 2025

Revised: 18 February 2025

Accepted: 25 February 2025

Published: 26 February 2025

Citation: Zou, Y.; Xia, H.; Yang, X.; Li, P.; Yi, Y. Dynamics Model of a Multi-Rotor UAV Propeller and Its Fault Detection. *Drones* **2025**, *9*, 176. <https://doi.org/10.3390/drones9030176>

Copyright: © 2025 by the authors. Licensee MDPI, Basel, Switzerland. This article is an open access article distributed under the terms and conditions of the Creative Commons Attribution (CC BY) license (<https://creativecommons.org/licenses/by/4.0/>).

1. Introduction

Unmanned aerial vehicles (UAVs) are widely used in many fields, such as road inspection, aerial photography, agricultural plant protection, pollution monitoring, logistics and transportation, search and retrieval, and intelligent transportation systems, because they can efficiently perform a wide range of complex aerial tasks [1]. As the application fields of UAVs become increasingly extensive, their reliability and safety issues become more important. The thrust and energy limitations of vehicle systems make reliable health monitoring more challenging due to the need to meet the detection achieved with fewer sensors and less computational power [2].

As a key actuator of the UAV to generate lift, the propeller's health status directly reflects the stability and controllability of the aircraft. In the actual operation process, propellers are inevitably affected by fatigue, overload, or external environmental factors such as high temperature, wind, sand, sun, precipitation, corrosion, and physical collision, which often lead to their failure. This may affect flight stability, cause the UAV to crash, or even result in casualties. Wild et al. [3] reported that equipment failures cause 64% of accidents and incidents involving remote-controlled UAVs, and fault detection is the first step in mitigating the effects of failures. Therefore, the study of fault detection methods for propellers has an important application value to ensure the safety and reliability of

the vehicle. In particular, the risk of losing control is especially prominent in quadrotor UAVs due to the lack of redundancy design, and effective measures are urgently needed to enhance their reliability and safety [4].

However, UAV fault diagnosis faces many challenges, mainly in the complexity of the system and the diversity of fault modes. Because UAVs are composed of multiple subsystems and have a wide range of fault types, the diagnostic process needs to comprehensively consider the interactions of different subsystems and fault characteristics. In addition, the real-time requirement is extremely high, especially when a fault occurs during flight, and a fast response is crucial. At the same time, the interference of external environmental factors and the problem of massive data processing also increase the difficulty of diagnosis. The limitations of multi-source data fusion and the lack of sufficient fault history data make traditional fault diagnosis methods more challenging. In addition, the complexity of human-machine collaboration needs to be effectively addressed in the fault diagnosis process. In recent years, model-based and signal-based approaches have been widely used in UAV fault detection. For example, Freddi et al. [5] proposed a model-based fault estimation method using a Thau observer, which is specifically designed for detecting sensor faults. Bazin et al. [6] introduced a direct measurement of individual thrusts for diagnostic purposes in which a quadrotor is equipped with a strain gauge at each actuator to directly measure the force generated by the propeller. This method is simple and intuitive and does not rely on the state of the system to estimate the motor thrust, but it requires the addition of multiple sensors and specialized circuits, which are costly and loaded for multi-rotors. Freddid et al. [7] constructed a dynamics model based on a six-degree-of-freedom rigid body under gravity and actuation to diagnose the residuals generated in a fault detection system, and the simulation analysis showed that this method can be applied to detect the sensor faults of a quadrotor UAV. Ortiz-Torres et al. [8] proposed an actuator fault based on an observer estimation of a linear and linear parameter varying proportional integral model and fault-tolerant control strategies for the vertical take-off and landing of UAVs. Under some specific assumptions, fault isolation and fault estimation are feasible for many types of faults. However, model-based approaches require significant modeling effort, and they conflict with the unavailability of many parameters in the application (e.g., lift and drag coefficients, inertia, and friction) [9]. In practice, the loss of effectiveness due to propeller damage may be completely masked by the variability in motor performance, leading to the failure of algorithmic model-based approaches [10]. For example, Liang et al. [2] proposed a novel fixed-wing UAV fault diagnosis framework for data-based approaches that takes into account process dynamics, multiple operating conditions, variable data density, and process disturbances to achieve a classified identification of a UAV actuator and sensor faults. Park et al. [11] proposed a deep neural network-based fault diagnosis algorithm for UAVs and extended the proposed method into a fault-tolerant controller to further improve flight reliability. The above methods do not need complex system models or assumptions about faults, but they require sufficient data to obtain the signals' characteristics and achieve fault detection [12]. Data-based methods require high computer arithmetic and often need a large amount of data to train the model. Notably, data acquisition often relies on layout sensors, which increase the UAV load and can affect the aerodynamic characteristics of the UAV, affecting flight stability. The installation of additional sensors will undoubtedly increase the detection cost of the UAV, even exceeding the manufacturing cost of small UAVs and losing detection value [13].

It is worth noting that acceleration signals are widely used in the fault diagnosis of rotating machinery [14,15] due to the better fault response characteristics of acceleration signals. However, vibration signals are usually not applied for feature extraction in UAV fault detection [16]. This is surprising because accelerometers are embedded in the flight

controller of almost every UAV, so vibration signals are easily accessible, and no additional sensors need to be installed. Therefore, in this study, we propose a UAV propeller fault detection method based on the signal analysis of the built-in inertial measurement unit (IMU). As is known, the built-in IMU of a UAV picks up typical multi-coupled signals, and determining how to separate and extract components rich in fault information is a key step to realizing fault detection. In this regard, we analyze the UAV propeller fault dynamics model to obtain the acceleration component with rich fault information. We achieve UAV propeller fault detection through the symmetrized dot pattern (SDP) algorithm, which has the advantages of a fast calculation speed and an obvious detection effect, and through the similarity quantization of normal and fault signals.

The main contributions of this study are as follows:

- (1) A dynamics model of UAV propellers in normal and fault states is constructed, providing a theoretical basis for propeller fault diagnosis.
- (2) A UAV propeller fault detection method without additional sensors and with fast response characteristics is proposed, which has important real-time fault detection application value.
- (3) The effectiveness of the proposed method is verified through simulation and experiments, and the experimental results are quantitatively evaluated using a similarity index.

The structure of this article is organized as follows: Necessary dynamics modeling is reviewed in Section 2. The theoretical basis of the algorithm and details of the proposed method are introduced in Section 3. The simulation and experimental analysis of the propeller failure dynamics model are introduced in Sections 4 and 5, respectively, using the proposed method. Conclusions are drawn in Section 6.

2. Modeling Multi-Rotor UAV Propeller Fault

This section briefly reviews the basic generation principle of multi-rotor acceleration and then analyzes the relationship between the acceleration signal of multi-rotor UAVs and the propeller's imbalance. Then, the acceleration components that are more sensitive to multi-rotor drone propeller faults are obtained through model analysis to provide a theoretical basis for multi-rotor drone propeller fault detection.

2.1. Multi-Rotor UAV Acceleration Analysis

A coordinate system is established with the multi-rotor as the center. The parts in the multi-rotor, including batteries, sensors, etc., are simplified, and the multi-rotor comes with N_x propellers with a total mass of m_i . Assuming that all propeller blades i on the multi-rotor are of equal dimensions, each propeller rotates with an angular velocity ω_i concerning the airframe and generates a thrust of magnitude f_i . Assuming a lift coefficient of K_f , the relationship between the thrust and angular velocity for each propeller can be expressed as in [17] as follows:

$$f_i = K_f \cdot \omega_i^2 \quad (1)$$

The multi-rotor may have some external perturbations during flight, such as aerodynamic perturbations, denoted by f_d , and the moving acceleration of the airframe can be expressed as follows:

$$m\ddot{x} = R e_3 \sum_i f_i - m_i g + f_d \quad (2)$$

where R denotes the rotation matrix that converts the angular velocity coordinate system of the airframe into inertial coordinates and the sum of the thrusts of the multi-rotor UAV. The effect of fault generation on acceleration is illustrated below to pave the way for simulation modeling and the interpretation of the algorithm.

2.2. Unbalanced Acceleration

During the flight process, the propeller of the multi-rotor may be damaged due to external disturbance. Assuming that the multi-rotor propeller is damaged in one or more places, the four-rotor is analyzed, as shown in Figure 1; the fault parts of the propeller are marked in red, and the fuselage frame is defined with the ternary groups e_1 , e_2 , and e_3 .

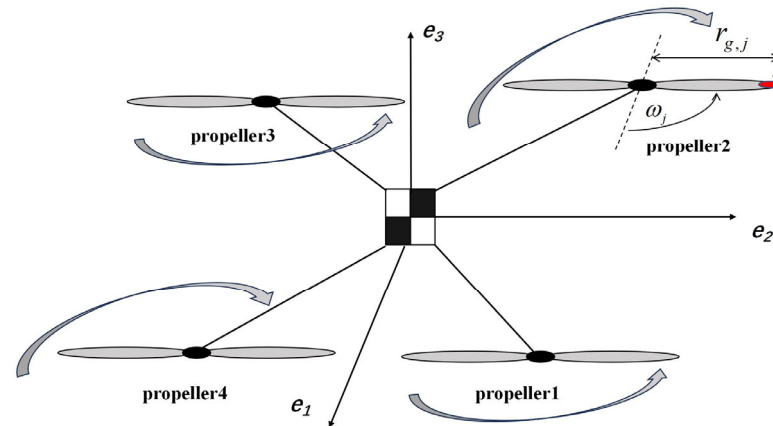


Figure 1. The quadrotor model with a damaged propeller.

Assuming that the propeller has an unbalanced mass $m_{g,j}$ at a distance $r_{g,j}$ from the center of rotation, it can be thought of as adding a negative mass to the damage of the propeller or a positive mass to the opposite side of the propeller. The angle of this imbalance with respect to the direction of e_3 is θ_3 , and the angle of the imbalance projected in the plane with respect to the direction of e_1 is θ_1 , corresponding to an angular velocity of ω_j .

The rotating unbalanced mass is small relative to the mass of the entire paddle. This corresponds to a small angle between the resulting unbalanced thrust and the e_3 axis, which can be approximated as a radial force generated on the e_3 axis and transmitted to the body of the multi-rotor, denoted as $f_{g,j}$ in the body coordinate system, written as follows:

$$f_{g,j} = m_{g,j} r_{g,j} \omega_j \begin{bmatrix} \sin \theta_3 \cos \theta_1 \\ \sin \theta_3 \sin \theta_1 \\ \cos \theta_3 \end{bmatrix} = \frac{m_{g,j} r_{g,j}}{K_f} f_j \begin{bmatrix} \sin \theta_3 \cos \theta_1 \\ \sin \theta_3 \sin \theta_1 \\ \cos \theta_3 \end{bmatrix} \quad (3)$$

Inside the built-in IMU of the multi-rotor contains an accelerometer that can be used to measure the fixed acceleration of the multi-rotor. This fixed acceleration is related to the force acting on the multi-rotor and the total mass, m_i , of the multi-rotor. It can be expressed as in [9] as follows:

$$a = \frac{1}{m_i} \left(\sum_i f_i + \sum_j f_{g,j} + f_d \right) + S_a \quad (4)$$

where S_a denotes the additional noise of the accelerometer; f_d denotes the external disturbance force acting on the multi-rotor in addition to the propeller and the mass of the multi-rotor. During the multi-rotor's flight, the value of the multi-rotor accelerometer will keep increasing and decreasing due to the additional noise and external interference force. Assuming that the IMU of the multi-rotor drone is mounted close enough to the multi-rotor drone's center of gravity, the angular velocity or angular acceleration of the multi-rotor will not significantly affect the acceleration. It is assumed that the body is rigid and there is no

vibration inside the multi-rotor. Separating the accelerometers at e_1 , e_2 , and e_3 (x -, y -, and z -axes) yields the following:

$$\begin{cases} a_x = \sum_j \left(\frac{m_{g,j} r_{g,j}}{m_i K_f} f_j \sin \theta_3 \cos \theta_1 \right) + \frac{1}{m_i} f_{d,x} + S_{a,x} \\ a_y = \sum_j \left(\frac{m_{g,j} r_{g,j}}{m_i K_f} f_j \sin \theta_3 \sin \theta_1 \right) + \frac{1}{m_i} f_{d,y} + S_{a,y} \\ a_z = \sum_j \left(\frac{m_{g,j} r_{g,j}}{m_i K_f} f_j \cos \theta_3 \right) + \frac{1}{m_i} \sum_i f_i + \frac{1}{m_i} f_{d,z} + S_{a,z} \end{cases} \quad (5)$$

where the angle of θ_3 is small, so $\cos \theta_3$ is much larger than the value of $\sin \theta_3$. Then, after the decomposition of the plane in the e_1 and e_2 directions, it can be seen that the amplitude of the vibration caused by the damage to the propeller in the e_3 direction is much larger than that of e_1 and e_2 . The impact of the damage to the propeller is more obvious in the e_3 direction, so it is important to isolate and extract the acceleration signals of the e_3 direction and carry out fault detection based on those signals. Therefore, the separation and extraction of the acceleration signal in the e_3 direction and fault detection based on this signal play an important role in realizing propeller fault detection.

3. Algorithms

3.1. SDP Algorithm

The principle of the SDP [18] is to transform the time-domain signal acquired by the sensor into a two-dimensional image in polar coordinates through the corresponding formula, and the fault information of the signal is expressed through the difference in the image. The SDP algorithm establishes the mapping relationship between Cartesian coordinates and polar coordinates based on the k th value and the $(k + 1)$ th value in the discrete-time series. It presents the signal as a symmetrical snowflake graph [19], and the basic schematic is shown in Figure 2.

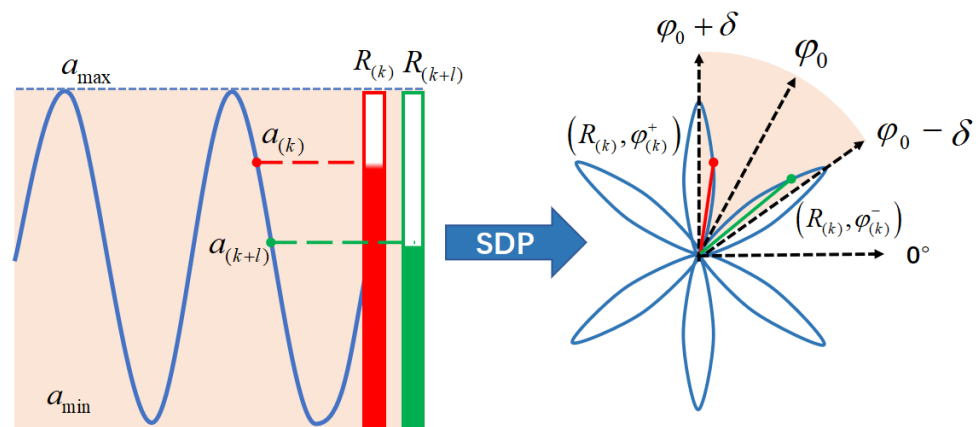


Figure 2. Principles of SDP.

The SDP can be expressed as in [19] by the following:

$$R^{(k)} = \frac{a_k - a_{\min}}{a_{\max} - a_{\min}} \quad (6)$$

$$\varphi_{(k)}^+ = \varphi_0 + \frac{a_{k+1} - a_{\min}}{a_{\max} - a_{\min}} \delta \quad (7)$$

$$\varphi_{(k)}^- = \varphi_0 - \frac{a_{k+1} - a_{\min}}{a_{\max} - a_{\min}} \delta \quad (8)$$

where $R_{(k)}$ and $\varphi_{(k)}$ denote the polar radius and angle of the k th value, respectively. a_{max} denotes the maximum of the signal, a_{min} denotes the minimum amplitude, a_k denotes the k th value, l is the hysteresis coefficient, and δ is the angular amplification factor.

With the above variations, the resulting polar value points may be repeated several times to cover the polar region. Still, the number of repetitions is not so excessive as to produce an overlapping loss of features. The raw signals of the propeller blades in the faulty state exhibit higher dispersion compared to the raw signals of the propeller blades in the normal state. It is difficult to distinguish the raw signals from the original signal, and applying the SDP algorithm can effectively amplify and visualize the differences to more precisely reveal the fault characteristics. This processing method significantly improves the recognizability of fault signals and provides strong support for fault diagnosis. Therefore, the SDP can be used to process the information collected from the multi-rotor to realize fault detection.

The fault detection algorithm proposed in this study has significant advantages. First, it does not require the installation of additional sensors, which can effectively reduce the hardware cost and simplify the system's structure. Second, the algorithm is less dependent on historical data, which enhances its adaptability in practical applications, and it can detect the fault status of UAVs in real time, thus significantly improving monitoring efficiency. In addition, the algorithm can show strong robustness and ensure the accuracy and stability of the fault detection results even when there is some external interference. These features give the algorithm a wide range of potential applications in the field of UAV fault diagnosis, especially in complex or dynamic operating environments.

3.2. Similarity Indicator

In practice, fault detection is usually accomplished through an empirical analysis of the rotationally symmetric image obtained by SDP calculation. To quantitatively evaluate the generated rotationally symmetric images, the similarity index is evaluated. First, the binary matrix is obtained through the grayscaling and binarization of the resulting image. Then, the effectiveness of the diagnosis is evaluated by comparing the similarity of the matrices. Graying involves dividing the image into several small regions, and each region is considered as a pixel. A grayscaled matrix is obtained after the pattern is grayscaled with the following expression:

$$H = (h_{mn})_{M \times N} \quad (9)$$

where H is the matrix of the pattern after grayscaling; M and N are the numbers of rows and columns of the H matrix; and h_{nm} is the grayscale value of the pixel in the n th row and the m th column, and its value ranges from 0 to 255.

The aim of the OTSU algorithm is to divide the whole pattern into two parts according to the grayscale characteristics: the graphic and the background. The proportion of foreground points in the image is w_0 , and the average grayscale is h_0 ; the proportion of background points in the image is w_1 , the average grayscale is h_1 , the total average grayscale of the image is h_g , and the variance σ of the foreground and background images is given by the following:

$$u = w_0 \times h_0 + w_1 \times h_1 \quad (10)$$

$$g = w_0 \times (h_0 - h_g)^2 + w_1 \times (h_1 - h_g)^2 \quad (11)$$

Combining the above two equations results in the following:

$$g = w_0 \times w_1 \times (h_0 - h_1)^2 \quad (12)$$

When the variance, g , has the maximum value, the difference between the foreground and background can be considered the maximum, and the grayscale τ is the optimal threshold at this time.

The converted grayscale matrix is converted to a binary matrix containing only 0 and 1 by setting a threshold value, where 0 denotes the background pixel and 1 denotes the pattern pixel (see Equation (10)). Equation (11) is the converted binary matrix; here, the threshold value is selected based on the maximum between-class variance method.

$$g_{mn} = \begin{cases} 0 & h_{mn} < \tau \\ 1 & h_{mn} \geq \tau \end{cases} \quad (13)$$

$$G = (g_{mn})_{M \times N} \quad (14)$$

where τ is the binarization threshold, which is calculated using the OTSU algorithm, g_{mn} is the binarized value of h_{mn} (containing only 0 and 1), and G is the binary matrix.

The maximum between-class variance method is used to divide the entire pattern into graphic and background parts based on the grayscale properties. The correctness of splitting the pattern into the background and graphic is higher when the inter-class variance between the target and background is larger. By calculating the between-class variance within each gray value, the maximum between-class variance value is taken as the threshold value.

After obtaining the binary matrix of the SDP, the diagnostic effect of the fault is expressed by comparing the similarity between the binary matrix of the unknown fault signal and the binary matrix of each known fault. Here, the Pearson correlation coefficient r is introduced to measure the degree of similarity between the two matrices, the absolute value of which is between 0 and 1. A smaller value indicates that the degree of similarity between the two matrices is lower. The bigger the difference between the normal and fault, the better the SDP algorithm is, and the r value is expressed by the following equation:

$$r = \frac{\sum_m \sum_n (A_{mn} - \bar{A})(B_{mn} - \bar{B})}{\sqrt{\left(\sum_m \sum_n (A_{mn} - \bar{A})^2\right) \left(\sum_m \sum_n (B_{mn} - \bar{B})^2\right)}} \quad (15)$$

where \bar{A} denotes the sample mean of A ; \bar{B} denotes the sample mean of B ; A_{mn} represents the value of sample A in m columns and n rows; and B_{mn} represents the value of sample B in m columns and n rows.

In the SDP algorithm, the snowflake diagram obtained by calculation relies on the empirical judgment of whether a fault occurs, while this study proposes a method to quantitatively evaluate the detection results by using similarity indexes, which not only enhances the robustness but also provides a more solid theoretical foundation and prospect for the practical application of the algorithm.

3.3. Propeller Fault Detection Methods

The flowchart for multi-rotor UAV propeller fault detection with the dynamic model proposed in this paper is shown in Figure 3. The main steps are as follows:

- (1) When the multi-rotor drone performs a flight mission in an open environment, the data transmission module is utilized to transmit the flight data back to the ground station in real time. The real-time multi-coupled acceleration data received by the ground station is processed and optimized to effectively separate acceleration signals in all directions or those extracted from the multi-rotor drone simulation platform to provide accurate data support for subsequent dynamic analysis and fault diagnosis.
- (2) The desired acceleration values are extracted based on the decoupled data. This experiment mainly focuses on the acceleration values recorded inside the IMU signal, so the acceleration values are mainly analyzed in this step.

- (3) Visually distinguishable SDP patterns are formed. The one-dimensional time-domain signal is transformed into a snowflake image. In the SDP method, because the hysteresis coefficient and the angular magnification factor affect the image's presentation, the parameters $l = 2$ and $\delta = 35$ are chosen based on the principle of maximizing the image difference [20].
- (4) Finally, based on the shape and convergence of the snowflake map generated by the SDP algorithm, it is determined whether the UAV propeller blade is damaged or not.

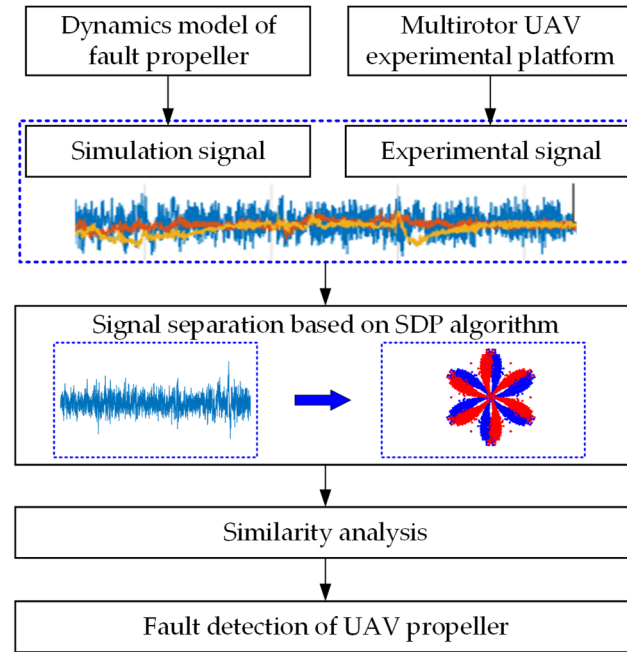


Figure 3. Flowchart of UAV propeller fault detection.

4. Simulation Analysis

4.1. Dynamics Simulation Model

To verify the effectiveness of the method proposed in this paper, a dynamics simulation model is used to validate the algorithm on the MATLAB R2022b platform [21]. This study focuses on the vibration of the UAV in different directions caused by the propeller failure, and the dynamics model of the multi-rotor UAV in the hovering state is considered to minimize the influence of the interference component on the vibration of the UAV. The effect of propeller failure and the external disturbance force are combined and replaced by one disturbance force, f . The dynamics model is established according to Equation (5):

$$\begin{cases} a_x = \frac{1}{m}\alpha_1 f_d + \beta S_a \\ a_y = \frac{1}{m}\alpha_1 f_d + \beta S_a \\ a_z = \frac{1}{m}\left(\sum_i f_i + \alpha_2 f_d\right) + \beta S_a - g \end{cases} \quad (16)$$

where α_1 and α_2 denote the influence factor of the disturbance force, and β denotes the accelerometer noise influence factor. Because the model considers the hovering state of the multi-rotor UAV, the angular velocity (ω_i) of the multi-rotor drone propeller is stable. Therefore, the acceleration model of the multi-rotor drone propeller in all directions, which was obtained by substituting Equation (1) into Equation (13), can be expressed as follows:

$$\begin{cases} a_x = \frac{1}{m}\alpha_1 f_d + \beta S_a \\ a_y = \frac{1}{m}\alpha_1 f_d + \beta S_a \\ a_z = \frac{1}{m}\left(\sum_i K_f \omega_i^2 + \alpha_2 f_d\right) + \beta S_a - g \end{cases} \quad (17)$$

The simulation parameters for the hovering state of multi-rotor drones are shown in Table 1.

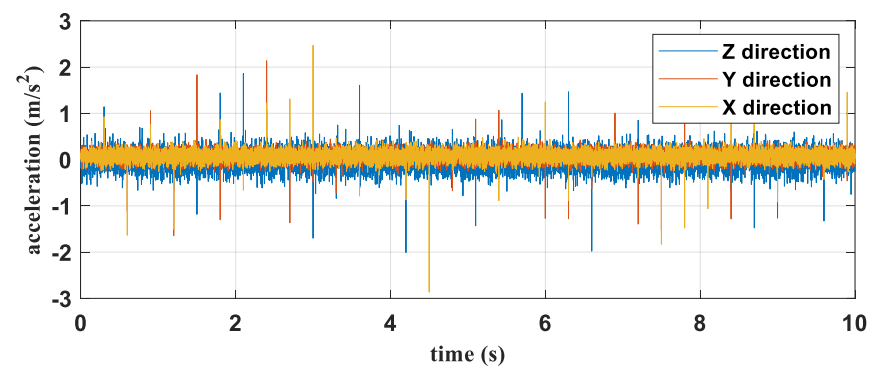
Table 1. Simulation parameters.

Parameter Name	Parameter Size	Parameter Name	Parameter Size
m_i/kg	1.5	α_1	0.02
$\sum_i f_i/\text{N}$	15	α_2	0.08
g	9.81	β	0.0039
$Kf/\text{N}/(\text{rad}\cdot\text{s}^{-1})^2$	10^{-6}	/	/

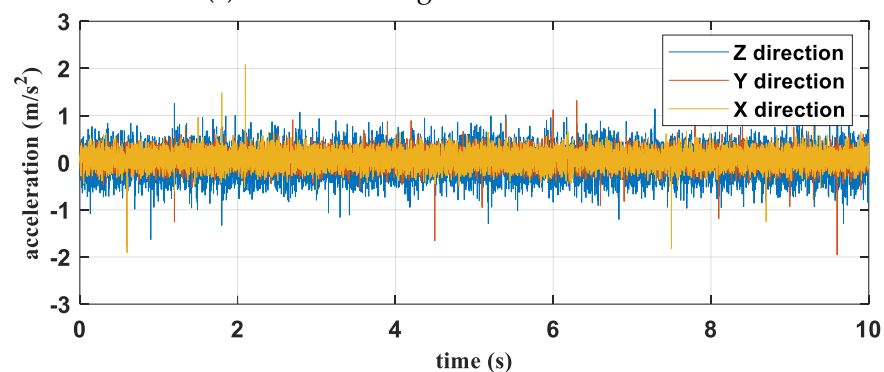
The values of S_a and f_d are randomly varied according to a normal distribution, and their variation range is set between -5 and 5 at the 100th variation, while the range of values for the rest of the time is limited to between -2 and 2 . Such a setup aims to more realistically simulate the actual situation during UAV flight, thus improving the accuracy and credibility of the model. It is worth noting that when the propeller fails, the disturbance force increases due to the unbalanced influence in the damaged part of the propeller. Therefore, the values of α_1 and α_2 can be increased to simulate the increase in the influence factor of the uncertain force, i.e., the amplitude of the vibration increases [22].

4.2. Analysis of Simulation Results

Based on the weight of the drone, the angular velocity of the quadcopter drone propeller in the hovering state can be calculated as $3872.98 \text{ rad}\cdot\text{s}^{-1}$. Then, the acceleration signals in the x , y , and z directions in the hovering state of the multi-rotor drone are obtained by substituting the parameters in Table 1 into Equation (13), as shown in Figure 4a. When the propeller fails, α_1 is 0.03, α_2 is 0.012, and the obtained acceleration in each direction is as shown in Figure 4b.



(a) acceleration signals for health states



(b) acceleration signal for fault condition

Figure 4. Simulation signals of different propeller states.

When comparing Figure 4a,b, it is difficult to recognize the acceleration change caused by the propeller fault from the acceleration signal. According to Equation (5), the acceleration signal in the z direction contains more fault information. The signals of the above two states are separated, and the acceleration signal in the z direction is shown in Figure 5. The amplitudes of the acceleration signals in Figure 5a,b are close to each other, and fault information cannot be detected. SDP calculations are performed on the normal and fault signals in the z-axis, respectively, and the results are shown in Figure 6a,b.

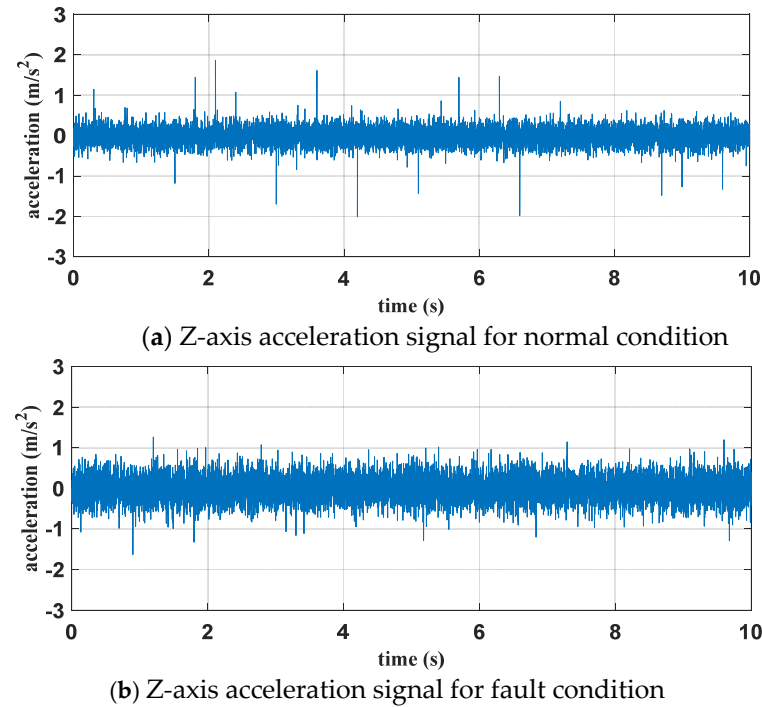


Figure 5. Acceleration signal in z-axis.

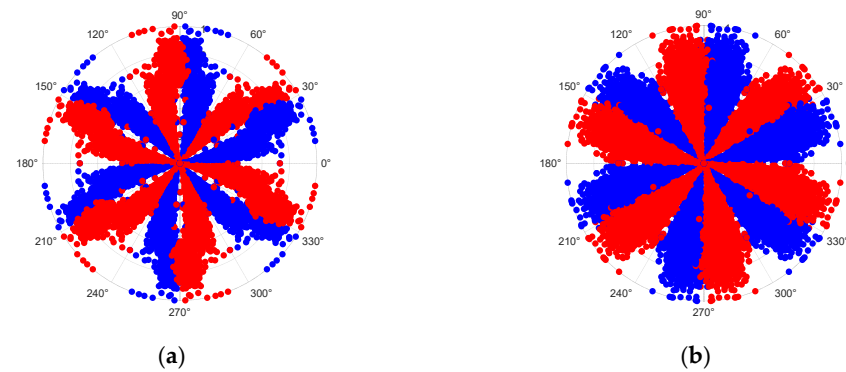


Figure 6. Results calculated using SDP. (a) Normal snowflake diagram; (b) faulty snowflake diagram.

Figure 5a shows that the snowflake map has a smaller fan blade thickness and a larger curvature, showing a uniform dispersion. Compared with Figure 5a, the outer thickness of Figure 5b is obviously larger than the center thickness, and the data are more discrete. Therefore, the proposed method can effectively detect propeller faults.

5. Experimental Analysis

5.1. Description of Experiment

To further verify the effectiveness of the proposed method in engineering, a quadrotor UAV platform is built based on F450, as shown in Figure 7. The relevant parameters of the equipment are shown in Table 2. The main flight controller PixHawk 2.4.8 chip used is STM32F427

(32-bit ARM Cortex M4 core with FPU 168 Mhz/256 KB RAM/2 MB Flash), MPU6000 is the main accelerometer and gyroscope, and an ST Micro 16-bit gyroscope, an ST Micro 14-bit accelerometer and compass (magnetometer), and MEAS barometer are also used.

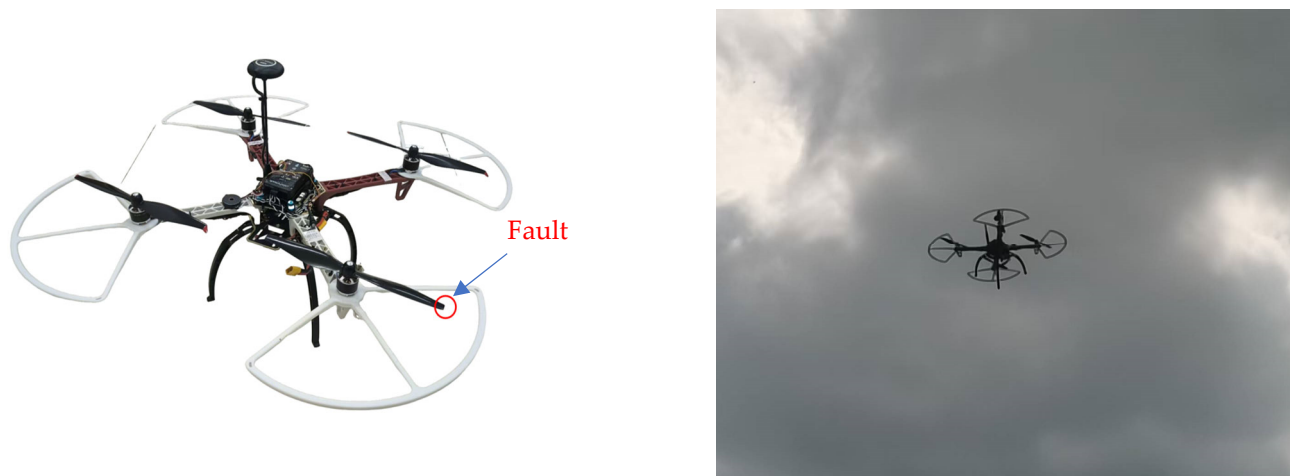


Figure 7. Multi-rotor drone test platform.

Table 2. Multiple rotor equipment parameters.

Parameter Name	Parameter Size
Flight Controller	PixHawk2.4.8
Rackmount	F450
Batteries	5200 mah
Rotary	1038 Paddle
Electrical Machinery	Langyu A2212 Brushless Motor
ESC	Lotte 20 A
GPS	M8n
Remote Controls	Lodi PRO
Firmware	Ardupilot (4.1.0)

The propeller failure was simulated by destroying the propeller blade tip, as shown in Figure 8. The dashed line delineates the propeller section of the disassembled unit, indicating that the damaged portion of the propeller has a mass of approximately 0.05 g, which constitutes about 0.44% of its total mass. Based on the above experimental equipment, the flight data in the hovering state of the multi-rotor drone are obtained under the same conditions of the flight environment (temperature, wind speed, and altitude) and the same multi-rotor drone control parameters when the multi-rotor drone propellers are normal and faulty, respectively.



Figure 8. The damaged propellers used in the experiments.

5.2. Experimental Results

Based on the above conditions, the acceleration values in the three directions are obtained with the z direction acceleration data for the normal and faulty states of the UAV,

as shown in Figure 9a,b. The value of the data recorded in the z-axis of the accelerometer of the multi-rotor is around -9.8 , and to make a visual comparison with the x- and y-axis data, the z-axis data are panned to the vicinity of zero. A total of 3000 points in the middle of the raw acceleration graphs were chosen to exclude the effect of the multi-rotor's vibration values during take-off and landing. When comparing Figure 9a,b, it is difficult to distinguish the acceleration change caused by propeller failure from the acceleration signal. The acceleration amplitudes in the x-, y-, and z-axis directions are close enough to detect the failure information. The results of the SDP calculations for normal and fault signals in the x, y, and z directions are shown in Figure 10.

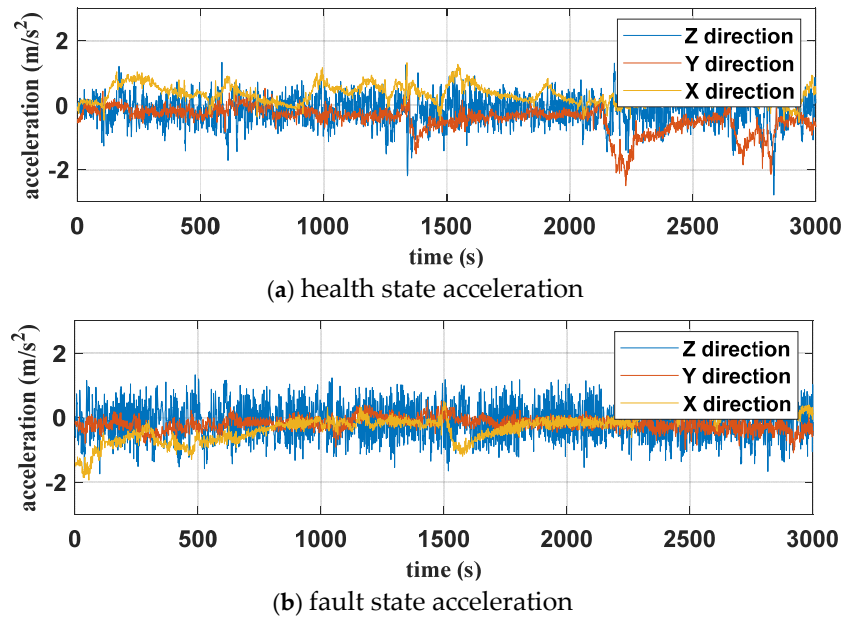


Figure 9. Acceleration signal of UAV.

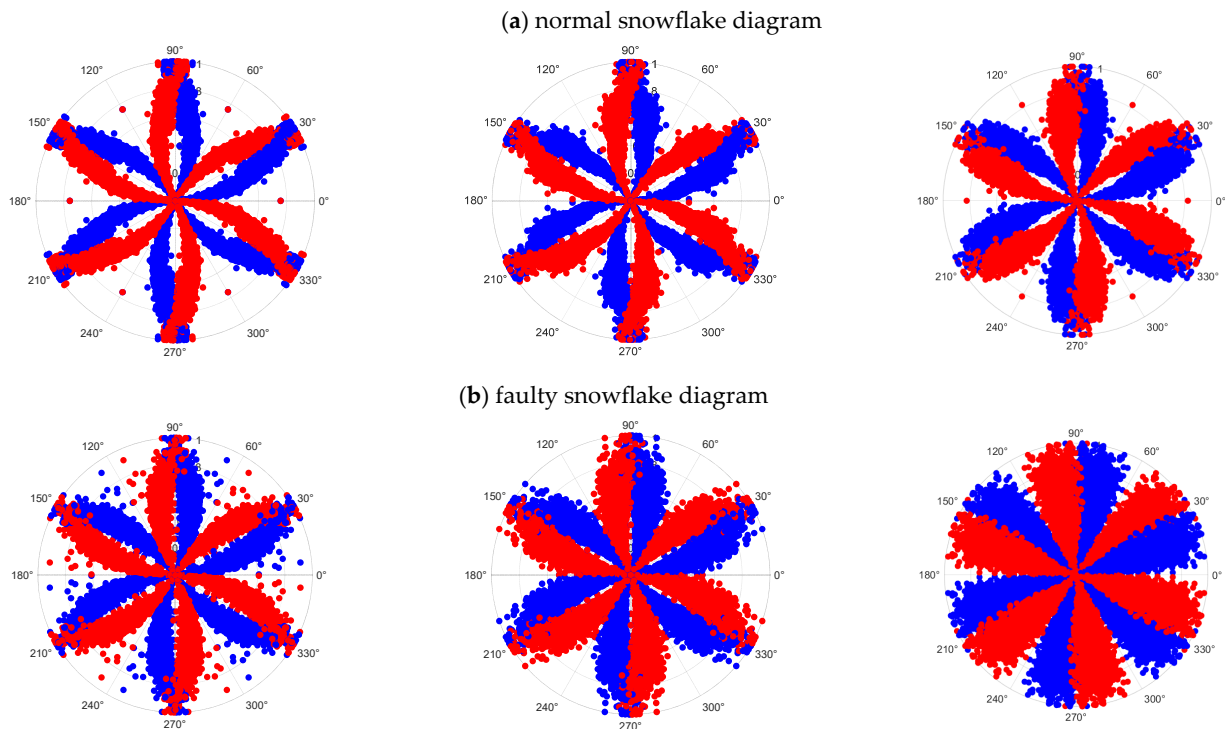


Figure 10. The snowflake diagrams of the experimental signals calculated using the SDP.

After being processed by the SDP algorithm, the morphological features of the snowflake graphs, including the curvature change and thickness, are different, and the snowflake graphs have better diagnosability compared with the original time-domain images. This proves the effectiveness of the proposed algorithm for the diagnosis of multi-rotor propeller faults.

Specifically, when the multi-rotor propeller is not damaged, the snowflake graph has a convergent shape with a gap in the middle, the snowflake petals are smooth with a small thickness, and the curvature varies greatly, similar to the shape of the propeller blade, which is shown in a typical normal snowflake graph. Compared with the normal snowflake graph, the fault snowflake graph, especially the z-axis, presents a dispersed shape due to the unbalanced force; the graph is uniform and full, the snowflake petals are similar to the fan, the thickness of the outer side is larger than the center thickness, and the transition is smooth. In summary, the SDP algorithm strengthens the overall expression of different motion states, and the individual characteristics are effectively weakened, showing the difference between normal and damaged propellers.

Although the difference between the feature point distributions can be recognized when comparing Figure 10a,b, the detector must evaluate the test or the supervisor's decision, and the application is limited. In this regard, we quantitatively evaluate the results of the SDP calculation based on the similarity index. A similarity calculation was performed according to the previous similarity index in the x, y, and z directions of the health state and fault state of the snowflake map, and the results are shown in Table 3. Table 3 shows that the similarity value of the z direction propeller is the smallest when in normal and faulty states, and the signal in the z direction contains richer fault information and is suitable for fault detection. This further verifies the correctness of the proposed theory. In addition, the indicator evaluation can obtain an objective and accurate threshold value, which overcomes empirical judgment, and it is more suitable for multi-rotor drone propeller fault detection.

Table 3. The results of the similarity quantification.

Direction	x	y	z
Degree of Similarity	84.37%	83.17%	76.20%

5.3. Future Research Directions

Although this experiment provided us with valuable experimental data and analysis results, its limitations should not be ignored. First, only the case of a single propeller tip with problems in the hovering state was considered in the experiment, and such an assumption may not comprehensively cover the effects of failures of different types of UAVs in different states, leading to some limitations in the applicability of the experimental results. In addition, only “quadrotor”-type UAVs were selected for the study; although this model is more common in the UAV field, with the continuous development of technology, more types of UAVs are now available on the market. These new models may have significant differences in design and performance compared to traditional quadcopters, so assessing more UAV models in future studies will help to further refine the experimental conclusions and enhance the broad applicability and accuracy of this study.

6. Conclusions

In this study, a propeller fault detection method based on the built-in IMU acceleration signal of a multi-rotor flight control system is proposed; it does not require the installation of additional sensors, which is conducive to reducing the detection cost, and it can be applied to realize real-time fault detection. Based on the dynamics analysis of propeller faults,

this study provides a theoretical basis for separating fault information-rich components from multiple coupled signals. The quantization of the SDP results using the similarity index further expands the application scope of the SDP algorithm. The simulation and experimental results show that the proposed method can effectively identify propeller faults in multi-rotor drones.

It is well known that fault detection results, if fed back to the multi-rotor drone control system, are of great significance to improve the performance of fault-tolerant control systems and ensure flight stability. In future work, research on the integration between accelerometers and microcontrollers will be strengthened to realize the further monitoring of multi-rotor drone propellers.

Author Contributions: Conceptualization, X.Y.; methodology, Y.Z.; software, Y.Y.; validation, H.X.; formal analysis, P.L.; investigation, Y.Z.; resources, Y.Z.; data curation, H.X.; writing—original draft preparation, Y.Z.; writing—review and editing, Y.Z.; visualization, X.Y.; supervision, H.X.; project administration, Y.Z.; funding acquisition, H.X. All authors have read and agreed to the published version of the manuscript.

Funding: This work was funded by the National Natural Science Foundation of China (12262015), the Yunnan Province Basic Research Special-Youth Project (202401AU070219), and the Science and Technology Projects of Yunnan Province’s Higher Education Institutions Serving Key Industries (FWCY-BSPY2024062).

Data Availability Statement: The data presented in this study are available upon request from the corresponding author.

Conflicts of Interest: The authors declare no conflicts of interest.

References

1. Lucic, M.C.; Bouhamed, O.; Ghazzai, H.; Khanfor, A.; Massoud, Y. Leveraging UAVs to Enable Dynamic and Smart Aerial Infrastructure for ITS and Smart Cities: An Overview. *Drones* **2023**, *7*, 79. [\[CrossRef\]](#)
2. Liang, S.; Zhang, S.; Huang, Y.; Zheng, X.; Cheng, J.; Wu, S. Data-driven fault diagnosis of FW-UAVs with consideration of multiple operation conditions. *ISA Trans.* **2022**, *126*, 472–485. [\[CrossRef\]](#) [\[PubMed\]](#)
3. Wild, G.; Murray, J.; Baxter, G. Exploring civil drone accidents and incidents to help prevent potential air disasters. *Aerospace* **2016**, *3*, 22. [\[CrossRef\]](#)
4. Suti, A.; Di Rito, G.; Galatolo, R. Fault-Tolerant Control of a Three-Phase Permanent Magnet Synchronous Motor for Lightweight UAV Propellers via Central Point Drive. *Actuators* **2021**, *10*, 253. [\[CrossRef\]](#)
5. Freddi, A.; Longhi, S.; Monteriu, A. A model-based fault diagnosis system for a mini-quadrotor. In Proceedings of the 7th Workshop on Advanced Control and Diagnosis, Zielona Góra, Poland, 19–20 November 2009; pp. 19–20.
6. Bazin, J.; Fields, T.; Smith, A.J. Feasibility of in-flight quadrotor individual motor thrust measurements. In Proceedings of the AIAA Atmospheric Flight Mechanics Conference, San Diego, CA, USA, 4–8 January 2016; p. 1760.
7. Freddi, A.; Longhi, S.; Monteriu, A. A diagnostic thau observer for a class of unmanned vehicles. *J. Intelligt Robot. Syst.* **2021**, *61*, 61–73. [\[CrossRef\]](#)
8. Ortiz-Torres, G.; Castillo, P.; Sorcia-Vázquez, F.D.; Rumbo-Morales, J.Y.; Brizuela-Mendoza, J.A.; De La Cruz-Soto, J.; Martínez-García, M. Fault estimation and fault tolerant control strategies applied to VTOL aerial vehicles with soft and aggressive actuator faults. *IEEE Access* **2020**, *8*, 10649–10661. [\[CrossRef\]](#)
9. Baldini, A.; Felicetti, R.; Ferracuti, F.; Freddi, A.; Iarlori, S.; Monteriù, A. Real-time propeller fault detection for multirotor drones based on vibration data analysis. *Eng. Appl. Artif. Intell.* **2023**, *123*, 106343. [\[CrossRef\]](#)
10. Ghalamchi, B.; Jia, Z.; Mueller, M.W. Real-time vibration-based propeller fault diagnosis for multicopters. *IEEE/ASME Trans. Mechatron.* **2019**, *25*, 395–405. [\[CrossRef\]](#)
11. Park, J.; Jung, Y.; Kim, J.H. Multiclass classification fault diagnosis of multirotor UAVs utilizing a deep neural network. *International Journal of Control.* *Autom. Syst.* **2020**, *20*, 1316–1326. [\[CrossRef\]](#)
12. Gangsar, P.; Tiwari, R. Signal based condition monitoring techniques for fault detection and diagnosis of induction motors: A state-of-the-art review. *Mech. Syst. Signal Process.* **2020**, *144*, 106908. [\[CrossRef\]](#)
13. Wang, B.; Shen, Y.; Zhang, Y. Active fault-tolerant control for a quadrotor helicopter against actuator faults and model uncertainties. *Aerosp. Sci. Technol.* **2020**, *99*, 105745. [\[CrossRef\]](#)

14. Hoang, D.T.; Kang, H.J. A survey on deep learning based bearing fault diagnosis. *Neurocomputing* **2019**, *335*, 327–335. [[CrossRef](#)]
15. Chakrapani, G.; Sugumaran, V. Transfer learning based fault diagnosis of automobile dry clutch system. *Eng. Appl. Artif. Intell.* **2023**, *117*, 105522. [[CrossRef](#)]
16. Fourlas, G.K.; Karras, G.C. A survey on fault diagnosis and fault-tolerant control methods for unmanned aerial vehicles. *Machines* **2021**, *9*, 197. [[CrossRef](#)]
17. Mahony, R.; Kumar, V.; Corke, P. Multirotor aerial vehicles: Modeling, estimation, and control of quadrotor. *IEEE Robot. Autom. Mag.* **2012**, *19*, 20–32. [[CrossRef](#)]
18. González, J.; Oro, J.M.F.; Delgado, L.; Mendez, D.; Argüelles, K.M.; Velarde-Suarez, S.; Rodriguez, D. Symmetrized dot pattern analysis for the unsteady vibration state in a Sirocco fan unit. *Appl. Acoust.* **2019**, *152*, 1–12. [[CrossRef](#)]
19. Tang, Y.; Zhang, X.; Qin, G.; Long, Z.; Huang, S.; Song, D.; Shao, H. Graph cardinality preserved attention network for fault diagnosis of induction motor under varying speed and load condition. *IEEE Trans. Ind. Inform.* **2021**, *18*, 3702–3712. [[CrossRef](#)]
20. Long, Z.; Xiaofei, Z.; Min, H.; Shoudao, H.; Guojun, Q.; Song, D. Motor Fault Diagnosis Based on Scale Invariant Image Features. *IEEE Trans. Ind. Inform.* **2021**, *18*, 1605–1617. [[CrossRef](#)]
21. Phadke, A.; Medrano, F.A.; Sekharan, C.N.; Chu, T. Designing UAV Swarm Experiments: A Simulator Selection and Experiment Design Process. *Sensors* **2023**, *23*, 7359. [[CrossRef](#)] [[PubMed](#)]
22. Dos Santos, D.A.; Yoneyama, T. A Bayesian solution to the multiple composite hypothesis testing for fault diagnosis in dynamic systems. *Automatica* **2011**, *47*, 158–163. [[CrossRef](#)]

Disclaimer/Publisher’s Note: The statements, opinions and data contained in all publications are solely those of the individual author(s) and contributor(s) and not of MDPI and/or the editor(s). MDPI and/or the editor(s) disclaim responsibility for any injury to people or property resulting from any ideas, methods, instructions or products referred to in the content.